

## Self-Assembly of Didodecyldimethylammonium Surfactants Modulated by Multivalent, Hydrolyzable Counterions

Connie K. Liu and Gregory G. Warr\*

School of Chemistry F11, The University of Sydney, Sydney, NSW 2006, Australia

### Supporting Information

**ABSTRACT:** The self-assembly behavior of double-chained didodecyldimethylammonium ( $\text{DDA}^+$ ) surfactants with hydrolyzable phosphate ( $\text{PO}_4^{3-}$ ,  $\text{HPO}_4^{2-}$ , and  $\text{H}_2\text{PO}_4^-$ ), oxalate ( $\text{HC}_2\text{O}_4^-$  and  $\text{C}_2\text{O}_4^{2-}$ ), and carbonate ( $\text{HCO}_3^-/\text{CO}_3^{2-}$ ) counterions was found to depend on both the counterion and its hydrolysis state, as determined by the pH of the system. Carbonate and phosphate ions at all hydrolysis states successfully stabilize an extended isotropic micellar solution region. These micelles are well-described as prolate ellipsoids which vary in size and aspect ratio depending on the surfactant concentration and hydrolysis state of the counterion. Both oxalate counterions form bilayer structures in dilute solution. The structures found with divalent oxalate,  $\text{C}_2\text{O}_4^{2-}$ , ions possessed very limited swelling capacity compared to the bilayer structures formed with monovalent oxalate,  $\text{HC}_2\text{O}_4^-$ , ions. The lamellar ( $\text{L}_\alpha$ ) phase was universally formed at sufficiently high surfactant concentrations for all hydrolyzable counterions. Two intermediate structures corresponding to a disordered mesh ( $\text{L}_\alpha^\text{D}$ ) and tetragonal ordered mesh (T) phase were found to form with  $\text{DDA}_2\text{HPO}_4$  prior to the  $\text{L}_\alpha$  phase but not with other phosphate counterions.



### INTRODUCTION

The structure of surfactant self-assemblies in micellar solutions and liquid crystalline phases is dictated by its molecular dimensions, hydrocarbon chain length ( $l_c$ ), volume ( $v$ ), and effective headgroup area ( $a_0$ ) through the packing parameter,  $v/a_0 l_c$ . In ionic surfactants, the counterion mediates electrostatic repulsions between headgroups and can significantly alter  $a_0$ . Surfactants with two alkyl tails, such as didodecyldimethylammonium ( $\text{DDA}^+$ ), typically have surfactant packing parameters in the range  $1/2 < v/a_0 l_c < 1$ , which favors the formation of lamellar phases ( $\text{L}_\alpha$ ) and other bilayer microstructures including vesicles and liposomes.<sup>1</sup>

Apart from fundamental interest,  $\text{DDA}^+$  surfactants have commercial, chemical, and pharmaceutical applications<sup>2–5</sup> and are implicated in biological self-assembly.<sup>6,7</sup> Much attention has been focused on  $\text{DDA}^+$  bromide,  $\text{Br}^-$  counterion (DDAB),<sup>8–13</sup> an insoluble surfactant that swells in water to form two  $\text{L}_\alpha$  phases.<sup>8</sup> In dilute solutions (< 3 wt %), a biphasic solution consisting of swollen lamellar crystallites dispersed in a metastable sponge phase,  $\text{L}_3$ , forms, which eventually becomes an isotropic micellar solution.<sup>10</sup>

On changing the counterion to hydroxide,  $\text{OH}^-$  (DDAOH), and acetate,  $\text{CH}_3\text{COO}^-$  (DDAAc), these surfactants are highly soluble in water and form clear solutions up to 1 M containing spontaneous vesicles and micelles.<sup>1,6,14–18</sup> The  $\text{L}_\alpha$  phase forms at higher concentrations.

This unusual behavior has been rationalized in terms of counterion binding to the surfactant headgroup and the stiffness of hydrocarbon chains which are modulated by headgroup interactions.<sup>17</sup> Comparing alkyltrimethylammonium

surfactants with  $\text{Br}^-$  and  $\text{OH}^-$ ,<sup>19</sup> the  $\text{OH}^-$  counterion is weakly binding and highly dissociated from the aggregate surface, causing the aggregates to be highly charged. This implies strong repulsions between aggregates, strong headgroup repulsion, and stiff chains for DDAOH. If chains are stiff, theory predicts that bilayers are able to form at  $v/a_0 l_c \sim 0.5$ .<sup>1</sup> In contrast, the  $\text{Br}^-$  counterion is more strongly binding, leading to less headgroup repulsions and more fluid chains within the DDAB bilayer. Furthermore, acetate counterions are hydrated by 6–7 waters and weakly bound to 4–5 more, and therefore, a relatively large headgroup area and strong electrostatic repulsions also exist for DDAAc.<sup>20</sup>

Recognizing the dramatic effects of different counterions on the phase behavior, Kang and Khan mapped out the complete binary phase diagrams for  $\text{DDA}^+$  associated with  $\text{CH}_3\text{COO}^-$ ,  $\text{OH}^-$  and completed the partial phase diagram for chloride  $\text{Cl}^-$  (DDAC) counterions,<sup>21,22</sup> previously described by Kunieda and Shinoda.<sup>2</sup> The effect of replacing monovalent counterions with a divalent sulfate,  $\text{SO}_4^{2-}$  (DDAS), counterion was also examined.<sup>21,22</sup> DDAC and DDAS are sparingly soluble in water, but like DDAB swell to form cloudy dispersions of bilayer structures in solution as well as homogeneous  $\text{L}_\alpha$  phases. Coexisting  $\text{L}_\alpha$  phases were not found in the  $\text{Cl}^-$  and  $\text{SO}_4^{2-}$  systems, but it was noted that the swelling capability of the  $\text{L}_\alpha$  phase is drastically reduced with the divalent  $\text{SO}_4^{2-}$  ion.

Received: July 24, 2014

Revised: August 30, 2014

Published: September 2, 2014

This phase behavior is again rationalized in terms of the affinity of the counterion to the surfactant headgroup. For relatively strongly binding counterions such as  $\text{Br}^-$  and  $\text{Cl}^-$ , the  $L_\alpha$  phase forms earlier and therefore has higher swelling capacity compared to the weaker binding counterions,  $\text{OH}^-$  and  $\text{CH}_3\text{COO}^-$ .<sup>23</sup> This trend is consistent with counterion binding strengths (and hydration) of alkyltrimethylammonium systems, where  $\text{OH}^- < \text{CH}_3\text{COO}^- < \text{Cl}^- < \text{Br}^-$ .<sup>17</sup>

Microstructures formed in  $\text{DDA}^+$  systems are modulated by the interplay of geometrical constraints and electrostatic interactions due to different counterions. Dubois and Zemb outline the seven possible microstructure transformations from ordered  $L_\alpha$  bilayers on dilution, emphasizing the richness in aggregation behavior despite the fact that some of these transformations have yet to be documented with strong experimental support.<sup>24</sup>

We have previously shown that hydrolyzable counterions stabilize highly curved, spherical micelles to such a degree that the hexagonally close-packed spheres (HCPS) micellar liquid crystal phase is universally observed in alkyltrimethylammonium salts.<sup>25,26</sup> This is realized even with counterions in multivalent hydrolysis states (e.g.,  $\text{HPO}_4^{2-}$ ,  $\text{C}_2\text{O}_4^{2-}$ ) because they remain strongly solvated and are unable to screen intramicellar headgroup repulsions that would allow micelles to grow into cylinders. These ions are thus expected to stabilize swollen lyotropic phases and possibly enable micelle formation by the double-chained, didodecyldimethylammonium analogues, as seen in hydroxide and acetate systems.<sup>1,6,14–18,21,22</sup>

## MATERIALS AND METHODS

Didodecyldimethylammonium surfactants with carbonate, phosphate, and oxalate anions were prepared by initially performing an ion exchange of the bromide salt (DDAB, 98% Fluka; used as received) to the hydroxide form using Amberlite IRA-400(OH) (Supelco) resin. The desired surfactant was then prepared by titration with an appropriate acid. The exact distribution of species and therefore the dominant counterion species depends on the final solution pH. Water used in all prepared solutions refers to Milli-Q water with a conductivity of  $18 \text{ M}\Omega \text{ cm}^{-1}$ . Didodecyldimethylammonium hydroxide (DDAOH) was prepared using previously reported methods.<sup>16,19,27,28</sup> The successful conversion of bromide to hydroxide was verified using electrospray ionization mass spectrometry analysis to confirm the absence of the bromide ion and  $(\text{DDA}^+)_n\text{OH}_n$  clusters.

Didodecyldimethylammonium phosphate ( $\text{DDAH}_2\text{PO}_4$ ,  $\text{DDA}_2\text{HPO}_4$ ,  $\text{DDA}_3\text{PO}_4$ ) and oxalate surfactants ( $\text{DDAH}_2\text{C}_2\text{O}_4$ ,  $\text{DDA}_2\text{C}_2\text{O}_4$ ) were prepared by titration of orthophosphoric acid (85%, Ajax Finechem) and oxalic acid (>99%, Ajax Finechem), respectively, to an appropriate equivalence of DDAOH solution. Didodecyldimethylammonium bicarbonate was prepared by adding a 2–3 blocks of dry ice to DDAOH solution. The pH (Mettler Toledo InLab Micro pH meter) of the initial hydroxide surfactant solutions was ~13 and the final solutions were ~6.5, indicating the successful neutralization of hydroxide ions. Clear, viscous solutions of didodecyldimethylammonium phosphates and bicarbonate were obtained while didodecyldimethylammonium oxalates were cloudy. A clear and colorless solution was formed on the addition of methanol to  $\text{DDAH}_2\text{C}_2\text{O}_4$  and  $\text{DDA}_2\text{C}_2\text{O}_4$ . All surfactants were freeze-dried and isolated as fine white powders. In solution, hydrolysis leads to a distribution of counterion species, which can be determined from the solution pH and the distribution of species calculated from their  $pK_a$ s (see Table S1 of Supporting Information). In almost all cases, the dominant equilibrium anion is the expected one from the titration. The exceptions are the carbonate salts, which are predominantly bicarbonate,  $\text{HCO}_3^-$  (and denoted as such henceforth), and phosphate, which contains 1%  $\text{PO}_4^{3-}$  but is predominantly  $\text{HPO}_4^{2-}$ . Nevertheless, we denote the most basic phosphate species  $\text{DDA}_3\text{PO}_4$

to differentiate from  $\text{DDA}_2\text{HPO}_4$ , which is predominantly  $\text{HPO}_4^{2-}$  but coexists with monovalent  $\text{H}_2\text{PO}_4^-$  rather than  $\text{PO}_4^{3-}$ . In no case is hydroxide a dominant anionic species.

Polarizing optical microscopy was performed on a Leica DM LB microscope fitted with cross polarizers, quarter-wave plate, and a DC 300 digital camera operating at room temperature. Concentration gradients were prepared by placing a small amount of solid surfactant sample onto a microscope slide, a coverslip pressed on top, and a few drops of water are added to the edge of the coverslip. Phases formed in the resulting concentration gradient after a few minutes are identified by their birefringence and optical textures.<sup>29–31</sup>

Small-angle X-ray scattering experiments were performed on the SAXS/WAXS beamline at the Australian Synchrotron, Victoria, Australia, following the gradient procedure employed previously.<sup>26</sup> In contrast with optical microscopy, here the concentration gradients and self-assembly phases form slowly and are stable for tens of hours. The resulting characteristic diffraction patterns are indexed, and the space group symmetry and consequently the structure of liquid crystalline phases are identified.<sup>31</sup>

Discrete samples were also prepared at fixed compositions (30–80 wt %) and examined visually by both polarizing optical microscopy and SAXS. SAXS patterns for discrete phase samples were collected on a SAXSess (Anton Parr) instrument using a  $\text{Cu K}\alpha$  X-ray source (1.54 Å), with point collimation and a  $q$ -range of  $0.02$ – $0.6 \text{ \AA}^{-1}$ . Scattered X-rays were collected on a phosphor image plate which was then scanned with a laser. Spectra were collected for 60 min at ambient temperature unless otherwise specified (~21 °C).

Small-angle neutron scattering (SANS) experiments were performed on the NG3 30 m beamline at the National Center for Neutron Research (NCNR), National Institute of Standards and Technology (NIST), Gaithersburg, MD.<sup>32</sup> 10% (w/v) stock surfactant solutions were prepared in deuterated water ( $\text{D}_2\text{O}$ ) (99.9%, Cambridge Isotope Laboratories).

Samples loaded into demountable quartz cells with 1 mm path length thermostated at 25 °C were used. Incident neutrons had an average wavelength of 6.0 Å and wavelength spread  $\Delta\lambda/\lambda$  of 0.124. Two sample-to-detector distances, 1.33 m (offset) and 8 m, were used, spanning a combined  $q$ -range of 0.0057–0.46  $\text{\AA}^{-1}$ . Raw SANS data were reduced to 1D data and fit in Igor Pro 6.12A using the reduction and fitting procedures provided by NIST.<sup>33</sup> Scattering length densities were calculated for each surfactant, individual surfactant ions, and  $\text{D}_2\text{O}$  using the NCNR SLD calculator.<sup>34,35</sup> In the absence of density measurements for surfactants associated with phosphate, oxalate, and bicarbonate counterions, the density was assumed to be 1.

The absolute scaled scattering intensity  $I(q)$  as a function of the scattering vector  $\mathbf{q}$  was fit to as  $I(q) = \phi_v V \Delta\rho^2 P(q) S(q)$ , where  $q = (4\pi/\lambda) \sin(\theta/2)$ ,  $\lambda$  is the wavelength,  $\theta$  is the scattering angle,  $\phi_v$  is the volume fraction,  $V$  is the volume of the particle, and  $\Delta\rho$  is the scattering length density difference between the micelle and the solution. The form factor,  $P(q)$ , describing the shape and size of the scattering body and structure factor,  $S(q)$ , describing interparticle interactions, were modeled for various trial micelle shapes such as spheres, rods, disks, ellipsoids, core–shell particles, etc.,<sup>36</sup> and intermicellar potentials such as hard sphere, sticky sphere, and screened Coulomb.<sup>37</sup>

## RESULTS AND DISCUSSION

The counterion and its charge/hydrolysis state were found to strongly affect the self-assembly patterns of didodecyldimethylammonium surfactants, leading to a diverse set of lyotropic liquid crystal phase and micellar solution structures.

An extensive, clear, isotropic ( $L_1$ ) solution phase was observed at concentrations up to at least 30 wt % with  $\text{PO}_4^{3-}$ ,  $\text{H}_2\text{PO}_4^-$ ,  $\text{HCO}_3^-$ , and 20 wt % with  $\text{HPO}_4^{2-}$  counterions. No isotropic solution phases were detected for  $\text{DDA}^+\text{HC}_2\text{O}_4^-$ , which formed a cloudy dispersion at 2 wt % in water. There is some evidence for an  $L_1$  phase in very dilute solutions of the  $\text{C}_2\text{O}_4^{2-}$  salt, described further below.

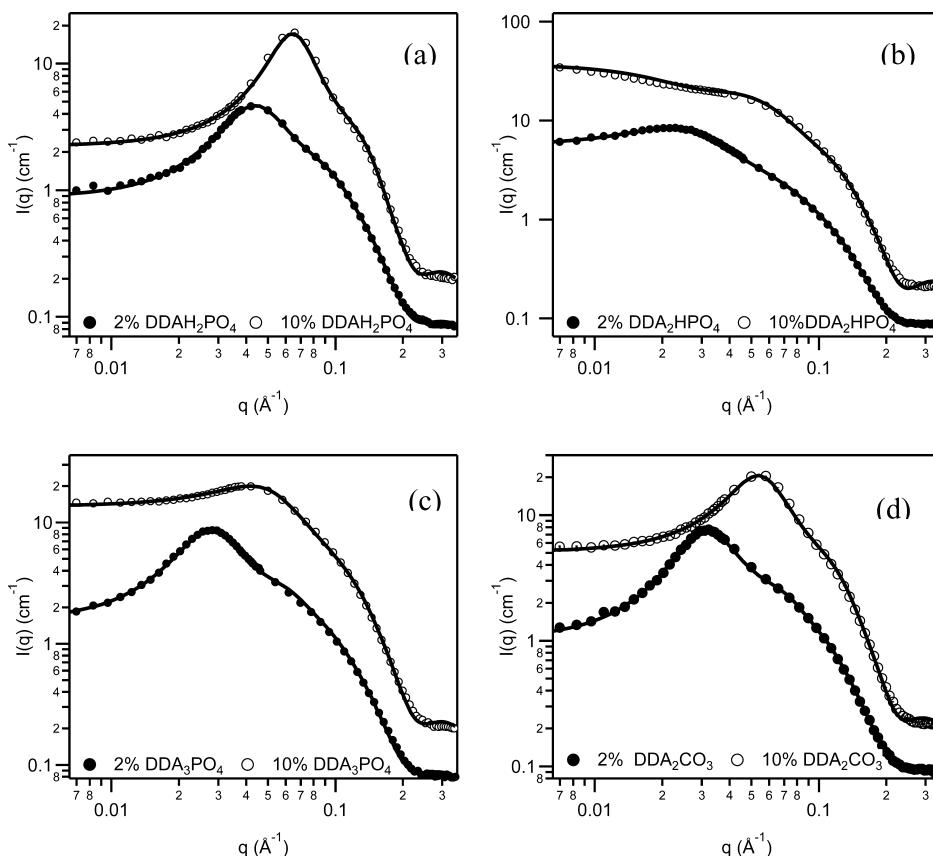


**Figure 1.** SANS patterns for 2 wt % (●) and 10 wt % (○) didodecyldimethylammonium phosphates: (a)  $\text{DDA}_3\text{PO}_4$ , (b)  $\text{DDA}_2\text{HPO}_4$ , (c)  $\text{DDAH}_2\text{PO}_4$ , and (d) didodecyldimethylammonium bicarbonate,  $\text{DDAHCO}_3$ . Solid lines are model fits to uniform spheroids for (a, c) and cylinders (b) with screened Coulomb repulsions.

This trend is consistent with our previous observations on micelle and lyotropic liquid crystal structures of single-tailed analogues of these surfactants; among these counterions, oxalate salts uniformly have the largest micelle aggregation numbers, indicating the strongest counterion association.<sup>25</sup> Similarly, hexadecyltrimethylammonium  $\text{HC}_2\text{O}_4^-$  was the only surfactant not found to exhibit a hexagonally close-packed spheres (HCPS) lyotropic phase.<sup>26</sup>  $\text{HC}_2\text{O}_4^-$  was found in both studies to be the counterion most like chloride in terms of the self-assembled structures formed.

**Isotropic Solution Phase.** Figure 1 shows SANS patterns together with model fits for 2 and 10 wt %  $\text{DDA}^+$  phosphate solutions at different states of hydrolysis and for  $\text{DDA}^+$  bicarbonate. The best fits (also shown) were achieved using model of homogeneous spheroids interacting through screened Coulomb repulsions.<sup>33,38</sup>

The best fit values for uniform spheroids with screened Coulomb interactions are listed in Table 1. The variable parameters include the micelle volume fraction,  $\phi$ , the rotational axis and cross-sectional radii of the spheroid,  $R_a$  and  $R_b$ , respectively, micellar charge, and ionic strength. The scattering length density (SLD) for the solvent was fixed to that of  $\text{D}_2\text{O}$ , and that of the ellipsoid was constrained to lie in an appropriate range to account for exchange of protons between the phosphate or bicarbonate counterions and deuterated solvent.

All  $\text{DDA}^+$  phosphates and bicarbonate are found to form uniaxially elongated structures or prolate spheroids ( $R_b < R_a$ ). Attempts to force oblate structures resulted in visibly poorer fits

**Table 1. SANS Best-Fit Parameters to a Model of Uniform Spheroids with Screened Coulomb Repulsions<sup>a</sup>**

surfactant sample	$\phi$	$R_a$ ( $\text{\AA}$ )	$R_b$ ( $\text{\AA}$ )	$R_a:R_b$	charge <sup>b</sup>	[salt] <sup>b</sup> (M)
2 wt % $\text{DDA}_3\text{PO}_4$	0.02	111.6	18.2	6	35	0.002
10 wt % $\text{DDA}_3\text{PO}_4$	0.10	121.3	18.2	7	12	0.008
2 wt % $\text{DDA}_2\text{HPO}_4$	0.02	148.2	17.8	8	21	0.003
10 wt % $\text{DDA}_2\text{HPO}_4$	0.10	138.0	17.0	8	0.006	0.008
2 wt % $\text{DDA H}_2\text{PO}_4$	0.02	54.2	17.4	3	24	0.004
10 wt % $\text{DDA H}_2\text{PO}_4$	0.11	66.5	17.7	4	26	0.006
2 wt % $\text{DDAHCO}_3$	0.02	93.7	17.7	5	27	0.005
10 wt % $\text{DDA HCO}_3$	0.10	96.0	17.7	5	19	0.021
2.7 wt % $\text{DDA OAc}^c$	55.2	17.8	3.1	18		
4.4 wt % $\text{DDA OAc}^c$	79.6	18.1	4.4	27		

<sup>a</sup>Volume fraction,  $\phi$ , radius of the rotational axis radius,  $R_a$ , cross-sectional radius,  $R_b$ , charge, monovalent salt concentration and the calculated aspect ratio of the prolate (rod) ellipsoid,  $R_a:R_b$ , for  $\text{DDA}^+$  phosphates and bicarbonate at 2 and 10 wt %. <sup>b</sup>Effective charge and ionic strength based on an assumed isotropic screened Coulomb potential (see text). <sup>c</sup>Acetate data from ref 14.

and significantly larger  $\chi^2$  values (at least 10 times higher). Fits to a cylindrical model yielded comparable micelle lengths ( $L \approx 2R_a$ ) and similar quality fits for the most elongated micelles, but we have used prolate spheroids to keep the same model for all aspect ratios and to facilitate comparison with  $\text{DDA}^+$  acetate.<sup>14</sup> The fitted volume fractions are consistent with the prepared concentrations; however, the values of the micelle charge and

salt concentration should be interpreted cautiously for such elongated structures, as the model assumes isotropic electrostatic interactions between spheres.

The fitted cross-sectional radii,  $R_b$ , are all slightly greater than a fully extended C<sub>12</sub> alkyl chain but are reasonable once the contribution from the dimethylammonium headgroup and counterions to the radii are included. The half-length or rotational axis radius of these rods,  $R_a$ , is particularly sensitive to the identity and hydrolysis state of the counterion. The micelles become more elongated as the average charge of the counterion is increased by hydrolysis from H<sub>2</sub>PO<sub>4</sub><sup>-</sup> to HPO<sub>4</sub><sup>2-</sup> and then decreased slightly with further increase in charge toward PO<sub>4</sub><sup>3-</sup>. DDAHCO<sub>3</sub> behaves similarly to the DDA<sup>+</sup> phosphates, yielding uniaxially elongated micelles with a similar cross-sectional radius. Its length is intermediate between monovalent and multivalent forms of phosphate.

For most of these systems the micelle length increases with concentration, as expected for cylindrical micelles. This was also reported previously for DDA<sup>+</sup> acetate micelles. DDA<sub>2</sub>HPO<sub>4</sub> is anomalous in that it appears to decrease somewhat in length on a 5-fold increase in concentration. (The same qualitative behavior is seen when the SANS patterns are fit to interacting cylindrical rather than spheroidal micelles.) This may be due to a failure of the approximation of isotropic interactions for such elongated structures. However, we interpret this as a real effect and tentatively ascribe it to the formation of branched micelles (see below).

The dilute isotropic phase of various soluble DDA<sup>+</sup> salts, including hydroxide, acetate, and other short-chained carboxylates, has been investigated in numerous studies.<sup>6,15,18,34</sup> Optical microscopy, cryo-TEM, and light scattering on DDA<sup>+</sup> hydroxide and acetate all show the presence of vesicles with sizes between 200 and 1000 Å, depending on dilution.<sup>6,15,18</sup> These have been reported to coexist with micelles, revealed by time-resolved fluorescence quenching, SANS, and NMR self-diffusion<sup>9,14,39</sup> or with a sponge (L<sub>3</sub>) phase, characterized by shear birefringence<sup>40</sup> and a broad SANS peak whose position is independent of concentration.<sup>10</sup> Some structural details remain unresolved in dilute solutions of DDA<sup>+</sup> salts. Very dilute solutions of DDA<sup>+</sup> salts can equilibrate extremely slowly, leading, for example, to a reported metastable L<sub>3</sub> sponge phase in very dilute DDAB solutions<sup>10</sup> and to spontaneous vesicles and a sponge phase in dilute DDA<sup>+</sup> acetate solutions.<sup>14,34,39</sup>

No vesicle dispersion in an L<sub>3</sub> phase was detected in any of the DDA<sup>+</sup> phosphate or bicarbonate systems. This may be because the concentration at which spontaneous vesicles are detected in other soluble DDA<sup>+</sup> surfactants is much lower than those used here (2–80 wt %). For DDAc, vesicles and L<sub>3</sub> appear at 0.5–1 wt %<sup>9</sup> and up to 0.56 wt % for DDAOH.<sup>15</sup> At concentrations above this, micelles are the predominant species in DDAc and DDAOH,<sup>6,15–18</sup> so other structures in phosphate or bicarbonate systems are unlikely to be detected.

SANS from DDA<sup>+</sup> acetate micelles under similar concentrations were consistent with prolate spheroids with very similar cross-sectional radii to those found in this study (see Table 1). Hydroxide is the weakest binding counterion reported for any quaternary ammonium surfactants. Based on aggregation numbers determined from fluorescence quenching, DDAOH micelles cannot be spherical either; they are expected to be prolate spheroids, but with an axial ratio <2.<sup>17</sup> The presence of micelles and a large L<sub>1</sub> phase in didodecyldimethylammonium phosphate and bicarbonate systems, as well as in hydroxide and carboxylates, is very different from expectations based on

bromide or chloride counterions. DDAB and DDAC are sparingly water-soluble and form only bilayer phases in solution. DDAB is even the archetype for adsorbed bilayers on hydrophilic substrates.<sup>41,42</sup> DDAB in particular has been extensively investigated, as it exhibits two coexisting lamellar phases, the more dilute of which can be diluted to 3 wt % before becoming a biphasic dispersion of vesicles in a dilute solution.<sup>10</sup>

We have previously shown that bicarbonate and phosphate counterions at various states of hydrolysis readily stabilize spherical micelles which are insensitive to added electrolyte<sup>25</sup> and that at high concentrations these form the otherwise rare HCPS liquid crystal phase, before forming a discrete cubic phase.<sup>26</sup> This was attributed to the strong solvation of these anions, which have been shown to exhibit weak selective binding to quaternary ammonium surfactant adsorbed layers in both 1- and 2-states.<sup>43</sup> Thus, despite the strong electrostatic binding of the HPO<sub>4</sub><sup>2-</sup> and PO<sub>4</sub><sup>3-</sup> forms to the micelle surface, this hydration layer prevents them from penetrating between the adjacent head groups and screening repulsions. Hence, the area per molecule at the micelle surface is unaffected by increased counterion concentration and the preferred packing condition continues to favor spheres.

The corresponding effect in double-chained surfactants similarly leads to micelle formation. Although lamellar phases are commonly observed with chloride and bromide counterions, the surfactant packing parameter for DDAB has been estimated to be 0.62.<sup>8</sup> This is consistent with expectations for bilayers ( $\frac{1}{2} < v/a_0 l_c < 1$ ),<sup>1</sup> but far below the “ideal” value of  $v/a_0 l_c = 1$ . Despite their large chain volume, in fact only a modest increase in area per molecule should be sufficient to meet the packing condition for cylindrical micelles ( $\frac{1}{3} < v/a_0 l_c < \frac{1}{2}$ ).<sup>15</sup>

Using micelle axial ratios as a proxy for the strength of intimate binding (and capacity to lower the molecular area), we find the order of binding to micelles to be OH<sup>-</sup> < OAc<sup>-</sup>, H<sub>2</sub>PO<sub>4</sub><sup>-</sup> < HCO<sub>3</sub><sup>-</sup> < PO<sub>4</sub><sup>3-</sup> < HPO<sub>4</sub><sup>2-</sup>. The phosphate binding sequence does not increase simply with charge, suggesting that there is a competition between the Coulomb attraction between cations and anions, and the strength of anion solvation such that the divalent HPO<sub>4</sub><sup>2-</sup> is most tightly bound to the micelle surface. This would explain the smaller stability range of the L<sub>1</sub> phase of DDA<sub>2</sub>HPO<sub>4</sub> compared with its 1- and 3-analogues as well as the fitted micelle shape and low apparent charge. It also explains some unusual lyotropic phases only found in DDA<sub>2</sub>HPO<sub>4</sub>.

**Lyotropic Phases.** 1. *DDA<sup>+</sup> Phosphates: Mesh Phases in DDA<sub>2</sub>HPO<sub>4</sub>.* Figure 2 shows the sequence of lyotropic phases observed in DDA<sup>+</sup> phosphates by polarizing optical microscopy. All DDA<sup>+</sup> phosphates, irrespective of the hydrolysis state of the phosphate counterions, at low concentrations form an extensive L<sub>1</sub> isotropic solution phase. In DDA<sub>3</sub>PO<sub>4</sub> and DDAH<sub>2</sub>PO<sub>4</sub>, streaky optical textures observed at high concentrations are consistent with L<sub>a</sub> phases. This was confirmed by SAXS measurements. Hydrated crystals are also apparent at the high concentration end of the L<sub>a</sub> phase of all three samples. However, DDA<sub>2</sub>HPO<sub>4</sub> exhibits additional optical textures between the L<sub>1</sub> and L<sub>a</sub> phases. The boundaries between the optical textures of these phases are indicated with lines for clarity in Figure 2. Higher magnification images showing the details of the intermediate phases between the L<sub>1</sub> and L<sub>a</sub> are shown in Supporting Information (Figure S1). Sharp boundaries between the textures are apparent, suggesting that these textures correspond to distinct, intermediate structures.

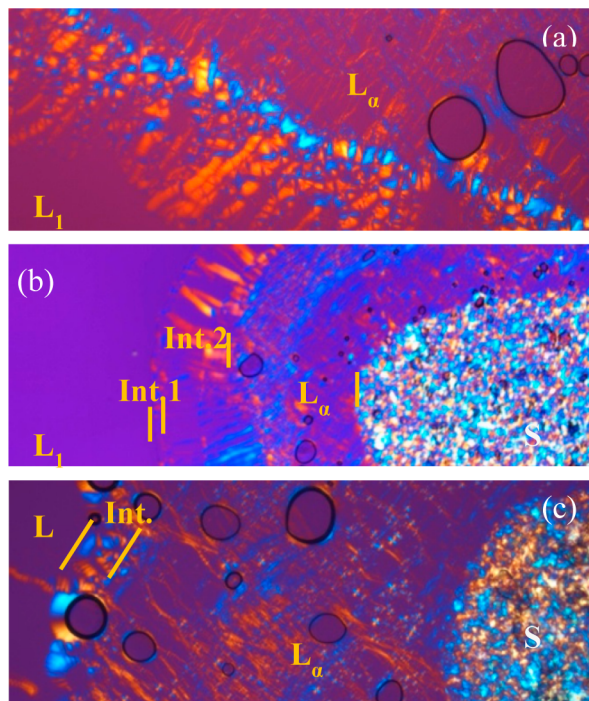


**Figure 2.** Polarizing optical micrograph of flooding experiments ( $10\times$ ) for (a)  $\text{DDA}_3\text{PO}_4$ , (b)  $\text{DDA}_2\text{HPO}_4$ , and (c)  $\text{DDAH}_2\text{PO}_4$ , showing optical textures from solid surfactant (S), lamellar ( $L_a$ ), intermediate (Int.), and isotropic (micellar) phases ( $L_1$ ). The surfactant concentration increases from bottom left to top right in (a) and left to right in (b) and (c).

Figure 3 shows selected synchrotron SAXS patterns obtained as a function of increasing concentration for  $\text{DDA}_2\text{HPO}_4$ . In

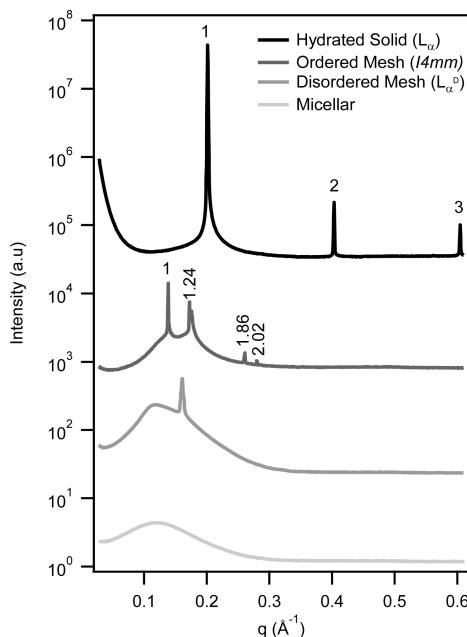


**Figure 3.** SAXS diffraction patterns showing the phase sequence for  $\text{DDA}_2\text{HPO}_4$  in a concentration gradient capillary scan. From bottom to top the concentration increases and phases are identified as micellar, disordered mesh phase ( $L_a^D$ ), tetragonal ordered mesh (T) ( $I4mm$ ), and lamellar ( $L_a$ ). The peak indices are indicated for the assigned liquid crystal phases. Curves are offset for clarity.

the most dilute region, a broad peak characteristic of interacting micelles in solution is seen. At higher concentrations this is followed by a single sharp peak at  $0.163 \text{ \AA}^{-1}$  together with a broad peak centered at  $0.120 \text{ \AA}^{-1}$ . This spectrum has previously been reported for a disordered mesh phase,  $L_a^D$ ,<sup>44–48</sup> consisting of a bilayer structure perforated with holes containing water that are weakly correlated. Here, the sharp peak arises from the regular bilayer spacing of  $38.5 \text{ \AA}$  and the additional diffuse peak from correlations between the water-filled holes in the plane of the bilayer. Note that the diffuse peak position is at lower  $q$  than the more dilute micelle solution and also that the sole sharp peak lies at higher  $q$  than the more concentrated phase above, which is also of different symmetry; these preclude the X-ray beam simply sampling two adjacent phases, but the diffraction pattern is consistent with the textures observed by polarizing optical microscopy.

At yet higher concentrations, a second intermediate phase scattering pattern is observed, consistent with the observation of two distinct optical textures by polarizing microscopy. This was found to index to a 3D body-centered tetragonal lattice, corresponding to the  $I4mm$  space group indicating the presence of an ordered “T” mesh phase with unit cell length  $a = 51.3 \text{ \AA}$ . This mesh structure is one of the two known ordered mesh phases.<sup>44,48</sup> Here, the water-filled defects are hexagonally arranged with respect to each other. The observed reflections are compared to the expected peak ratios for the  $I4mm$  space group in Table S2. While the possibility of these two intermediate phases being metastable cannot be ruled out, their rapid formation under the microscope and long lifetimes under synchrotron SAXS examination suggest that they are equilibrium phases.

At the highest concentration, where crystalline solid was also present, lamellar symmetry with peak ratio 1:2:3 is observed. The primary diffraction peak at  $0.201 \text{ \AA}^{-1}$  corresponds to a repeat spacing of  $31.2 \text{ \AA}$ . This is smaller than the ideal value of  $33.4 \text{ \AA}$ , suggesting that the hydrocarbon chains are not fully extended or are intercalated in the bilayer, but is consistent with previous data for DDAB.<sup>1,11</sup>

As found by polarizing optical microscopy (Figure 2), the SAXS patterns similarly obtained in a concentration gradient for  $\text{DDA}_3\text{PO}_4$  shows the presence of only two phases: interacting micelles in solution ( $L_1$ ) and a  $L_a$  phase at higher concentrations. This is consistent with the phase assignments from polarizing optical microscopy where no intermediate textures were observed.  $\text{DDAH}_2\text{PO}_4$  polarizing optical microscopy (Figure 2c) does also show an unusual optical texture, suspiciously like an intermediate phase, between  $L_1$  and  $L_a$  textures. This was not detected by SAXS, suggesting that it is stable only over a very narrow composition range (Figure S2).

Mesh structures are expected to form at intermediate values of the surfactant packing parameter,  $\frac{1}{2} < \nu/a_0 l_c \leq \frac{2}{3}$ .<sup>49</sup> Why are these only observed in  $\text{HPO}_4^{2-}$ ? Among the counterions examined here and previously that permit micelle formation of  $\text{DDA}^+$  salts,  $\text{HPO}_4^{2-}$  is the most strongly bound based on micelle shape, and on the concentration range of the  $L_1$  phase. Its ability to stabilize long uniaxial micelles is consistent with the branched cylinders or holey bilayer membranes that constitute meshes. More strongly binding counterions like sulfate, chloride, and bromide (and oxalate—see below) only stabilize bilayers, and the  $L_1$  phase is virtually absent. Thus,  $\text{HPO}_4^{2-}$  lies just at the correct balance point for intermediate phase structures to form. Branched phases should also be achievable by judicious choice of “intermediate” counterion

selectivity, but phosphates have the advantage of modulating curvature by a change in pH; one can readily imagine opening and closing pores in bilayers.

Mesh and other such intermediate structures are implicated in biological membrane self-assembly and the fine control of membrane topology through lipid biochemistry.<sup>7</sup> AFM experiments have demonstrated the presence of circular punctures in biologically relevant lipid bilayers, occupying 10–20% of the membrane area,<sup>50</sup> as well as in synthetic surfactant systems.<sup>51,52</sup> A series of studies using direct imaging by cryo-TEM also suggest the importance of such intermediate membrane structures in biological processes.<sup>53</sup> Potential topological and geometric control can be achieved through changes in the biochemistry within the vicinity of the bilayer, and thus punctures should be able to form reversibly in a controlled manner.<sup>7</sup>

**2. DDA<sup>+</sup> Oxalates.** In contrast to phosphate and bicarbonate surfactants, no extensive isotropic micellar solution phase was detected for DDA<sup>+</sup> oxalates. Instead, a transparent birefringent solution composed of highly swollen bilayers was found in DDAHC<sub>2</sub>O<sub>4</sub> up to 38 wt % in water, and an opaque L<sub>α</sub> liquid crystal phase was formed above 49.5 wt %. In dilute solution, from 2 wt % to at least 30 wt %, DDA<sub>2</sub>C<sub>2</sub>O<sub>4</sub> forms cloudy solutions similar to those of dilute solutions of DDAB.<sup>10</sup>

This low concentration behavior of DDA<sub>2</sub>C<sub>2</sub>O<sub>4</sub> is qualitatively similar to that reported for other insoluble DDA<sup>+</sup> systems, DDAB, DDAC, and DDAS beyond their lamellar swelling limit, where they form L<sub>α</sub> structures dispersed in a dilute solution or metastable sponge phase, L<sub>3</sub>. Their insolubility and formation of L<sub>α</sub> structures at such high dilution are again accounted for by the strength of counterion association to the surfactant head groups and the stiffness of the bilayer chains which are modulated by headgroup interactions.<sup>1,17</sup> We have previously shown using SANS on alkyltrimethylammonium systems that both the monovalent and divalent oxalate counterions have higher screening efficiency than hydroxide, bicarbonate, and phosphate but lower screening efficiency than chloride and bromide.<sup>25</sup>

Figure 4 contrasts the polarizing optical micrographs of the concentration gradient formed between water-DDA<sub>2</sub>C<sub>2</sub>O<sub>4</sub> and water-DDAH<sub>2</sub>O<sub>4</sub>. At high concentrations of both species, the optical textures are consistent with a L<sub>α</sub> phase and hydrated surfactant crystals. In C<sub>2</sub>O<sub>4</sub><sup>2-</sup>, lamellar oily streak textures grow slowly into the solvent as it is taken up by the surfactant L<sub>α</sub> structures.<sup>40</sup> In contrast, myelinic figures are seen in DDAHC<sub>2</sub>O<sub>4</sub>, which indicates the rapid and efficient swelling of the L<sub>α</sub> phase.<sup>54</sup>

Figure 5a shows the SAXS diffraction patterns for DDAHC<sub>2</sub>O<sub>4</sub> in a gradient capillary as a function of concentration or position. Figure 5b shows SANS patterns for dilute DDAHC<sub>2</sub>O<sub>4</sub> samples of known composition. At 10 wt % two broad peaks in the ratio of 1:2 are observed, which are similar to the most dilute SAXS pattern. This was fit to a lamellar paracrystal model<sup>55</sup> with best fit yielding a repeat spacing of 213 Å, a polydispersity of 0.19 over 28 correlated layers, and a bilayer thickness of 23.5 Å. This is consistent with the previously reported thickness of a DDAB membrane (24 Å) excluding the counterion.<sup>11</sup>

At 2 wt %, the scattering pattern is also consistent with locally lamellar structure, exhibiting the characteristic  $q^{-2}$  dependence below about 0.04 Å<sup>-1</sup> originating from the presence of bilayer sheets. The absence of Bragg diffraction peaks is typical for dilute, noninteracting, swollen vesicles,

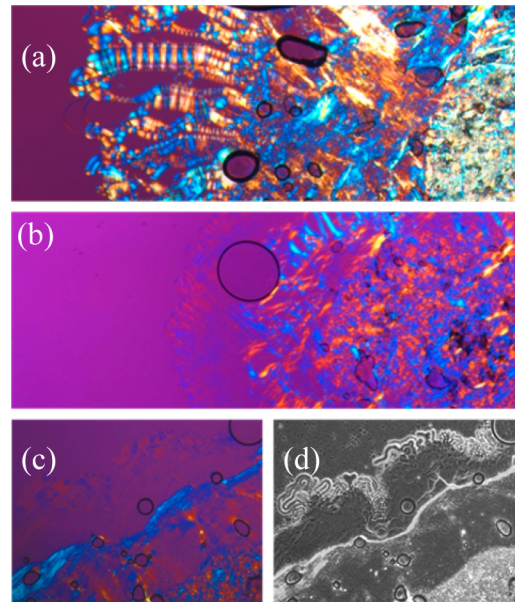


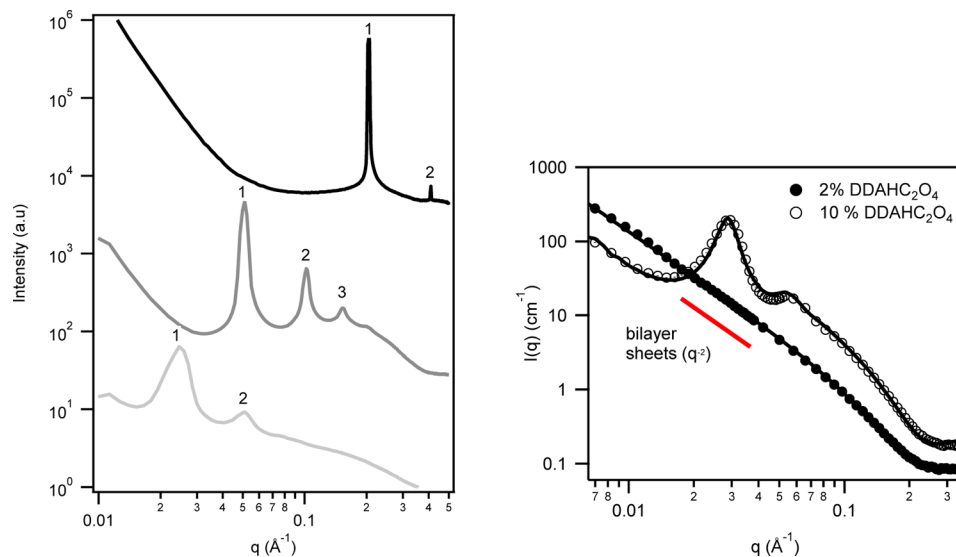
**Figure 4.** Polarizing optical micrographs of flooding experiments (5×) for (a) DDA<sub>2</sub>C<sub>2</sub>O<sub>4</sub> and (b) DDAHC<sub>2</sub>O<sub>4</sub>. The concentration increases from left to right. The details of the dilute region DDAHC<sub>2</sub>O<sub>4</sub> where the concentration increases from top left to bottom right are shown at higher magnification (10×) (c); an identical image without polarization and in grayscale to enhance myelinic figures is also shown (d).

although the predicted lamellar peak position based on dilution of the 10 wt % solution would be just below the accessible  $q$  range, so it cannot be completely ruled out.<sup>24</sup> From model fitting to a lamellar form factor, the bilayer thickness was found to be 20.1 Å with a polydispersity of 0.34.

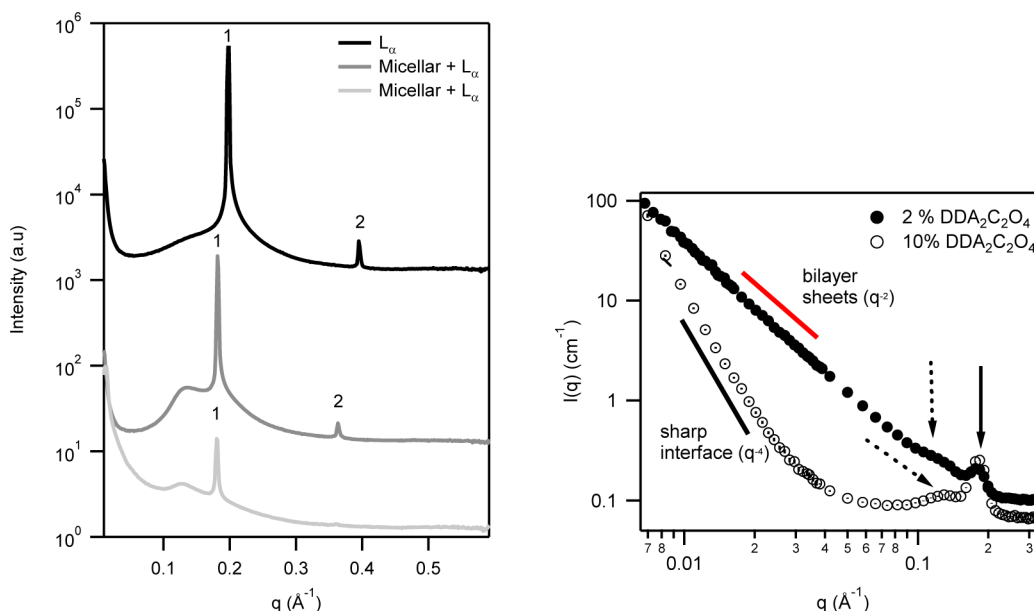
Using the bilayer thickness,  $2l$ , from SANS and the dilution law,  $\varphi = 2l/d$ , the surfactant volume fraction,  $\varphi$ , estimated from the repeat spacing,  $d$ ,<sup>56</sup> for each of the DDAHC<sub>2</sub>O<sub>4</sub> samples in Figure 5a, from top to bottom are 0.77, 0.19, and 0.11. The most dilute of these is close to the more concentrated sample examined by SANS. At higher concentrations the peaks become sharper as the bilayers become more ordered, and 4 orders of reflection are visible in the available  $q$  range at the intermediate concentrations.

Figure 6 similarly shows the SAXS diffraction patterns for DDA<sub>2</sub>C<sub>2</sub>O<sub>4</sub> in gradient capillaries and SANS patterns of dilute samples of known compositions. Both show a broad peak at low  $q$ , together with sharp diffraction peaks that index to a lamellar phase. (The SANS lamellar peaks are resolution limited by the wavelength spread in the neutron beam.) Unlike DDAHC<sub>2</sub>O<sub>4</sub>, the primary sharp (lamellar) diffraction peak at 0.1803 Å<sup>-1</sup> does not change with composition, except in the most concentrated sample shown at the top of Figure 6. This, together with the observed broad scattering peak that also remains a constant feature near 0.12, shows these samples to be biphasic, consisting of coexisting L<sub>α</sub> + L<sub>1</sub> (dilute micellar) phases of fixed compositions. This is consistent with poor swelling and optical textures observed in Figure 4 and peak ratios of 1:2 in Figure 6. Such biphasic solutions have also been observed in the dilute regions of poorly soluble DDA<sup>+</sup> surfactants with bromide,<sup>10</sup> chloride,<sup>2</sup> and sulfate<sup>21</sup> counterions as well as in various anionic surfactant-alcohol-brine<sup>40</sup> mixtures.

Using the bilayer thickness obtained for DDAHC<sub>2</sub>O<sub>4</sub> above and the peak position in the coexistence region, the coexisting



**Figure 5.** (a) SAXS diffraction patterns showing the phase sequence for  $\text{DDAHC}_2\text{O}_4$  in a concentration gradient capillary scan. The concentration increases from bottom to top, and  $L_\alpha$  structures are formed at all compositions. The peak indices are indicated by the numbers above. (b) SANS patterns for 2 wt % (●) and 10 wt % (○)  $\text{DDAHC}_2\text{O}_4^-$ . The solid lines are model fits to lamellar structures of which the bilayer thickness is a fit parameter. The solid red line shows the  $q^{-2}$  dependence, which is expected for bilayer sheets.



**Figure 6.** (a) SAXS diffraction patterns showing the phase sequence for  $\text{DDA}_2\text{C}_2\text{O}_4$  in a concentration gradient capillary scan. From bottom to top the concentration increases, a micellar ( $L_1$ ) solution in coexistence with lamellar ( $L_\alpha$ ) structures is present in the dilute region, and a pure  $L_\alpha$  phase is seen in the concentrated region. Curves are offset for clarity. (b) SANS patterns for 2 wt % (●) and 10 wt % (○)  $\text{DDA}_2\text{C}_2\text{O}_4$ . The solid red line shows the  $q^{-2}$  dependence which is expected for sheets, and the solid black line shows the  $q^{-4}$  dependence expected for sharp interfaces due to the presence of particles. The solid arrow indicates the primary diffraction peak observed for  $L_\alpha$  bilayers, and dashed-line arrows indicate the diffuse peak due to a second phase of interacting micelles in solution.

composition (maximum swelling) of the  $\text{DDA}_2\text{C}_2\text{O}_4$  lamellar phase is estimated to be  $\varphi = 0.67$ . The primary diffraction peak for the isolated  $L_\alpha$  phase sampled is at  $0.198 \text{ \AA}^{-1}$ , which corresponds to a bilayer repeat spacing ( $d$ ) of  $31.7 \text{ \AA}$  and a surfactant volume fraction of 0.74. Visual observation of an 80 wt % dilution showed  $L_\alpha$  coexisting with solid crystals, so that the  $\text{DDA}_2\text{C}_2\text{O}_4$  lamellar phase is only stable over a narrow range of compositions  $0.67 < L_\alpha < 0.8$ .

The broad peak indicated by dashed-line arrows in Figure 6b shows that the coexisting micellar phase is still detectable in the SANS spectra at 2 wt %  $\text{DDA}_2\text{C}_2\text{O}_4$ . However, it is somewhat

obscured by the intense  $q^{-2}$  power-law scattering at low angles that confirms the presence of bilayers. At 10 wt % the bilayer form-factor scattering is overwhelmed by the  $q^{-4}$  Porod-limit scattering at  $q < 0.02 \text{ \AA}^{-1}$ . This is attributed to scattering from the interface between dispersed, poorly swollen, multilamellar vesicles and the continuous (micellar) phase. At this composition, a polydisperse population of densely packed birefringent droplets is observed by optical microscopy (see Supporting Information Figure S3).

The lack of swelling in  $L_\alpha$  bilayers for  $\text{DDA}^+$  associated with  $\text{C}_2\text{O}_4^{2-}$  parallels that of  $\text{SO}_4^{2-}$ .<sup>21</sup> It has previously been

suggested that the inability to incorporate water between bilayers stabilized with divalent ions is due to an attractive electrostatic force between bilayers,<sup>57</sup> which is not present with monovalent ions.

The maximum  $L_\alpha$  swelling dimensions observed for  $\text{HC}_2\text{O}_4^-$  are comparable to those reported for  $\text{Cl}^-$  (less than 200 Å, or 12 wt % surfactant).<sup>13</sup> This contrasts with  $\text{Br}^-$  and  $\text{NO}_3^-$  salts, which can be swollen up to 1000 Å bilayer spacings, corresponding to only 2 wt % surfactant in solution.<sup>23</sup> Direct measurements of counterion selectivity in the lamellar phase as well as solution and phase behavior studies of the corresponding alkyltrimethylammonium chlorides and bromides show that this correlates well with counterion binding:  $\text{Cl}^-$  counterions are more weakly binding than  $\text{Br}^-$ .<sup>17,58–60</sup> This suggests that the counterion affinities of  $\text{HC}_2\text{O}_4^-$  and  $\text{Cl}^-$  for the  $\text{DDA}^+$  head groups are similar and that both are more strongly binding than the micelle-forming phosphate species.

**3.  $\text{DDAHCO}_3$ : Coexisting Lamellar Phases.** Polarizing optical micrographs for the flooding experiment for  $\text{DDAHCO}_3$  are shown in Figure 7. Two distinct optical textures are seen,

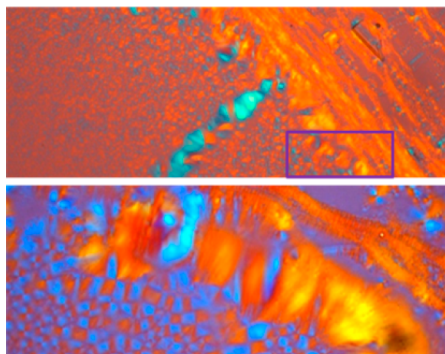


**Figure 7.** Polarizing optical micrograph of flooding experiment (20×) for  $\text{DDAHCO}_3$  (top). The concentration gradient increases from left to right. Details within the boxed region are viewed at higher magnification (50×) (bottom). Two different optical textures, both corresponding to  $L_\alpha$  are observed. In the dilute region, a mosaic texture is present whereas in the concentrated region, oily streaks and Maltese crosses are observed.

both corresponding to  $L_\alpha$  phases. Within the dilute region a mosaic texture is observed, whereas oily streaks and Maltese crosses are present at higher concentrations.

Figure 8 shows the SAXS diffraction patterns at two intermediate compositions in a concentration gradient capillary. In the lower, more dilute pattern (gray), the two peaks index to  $L_\alpha$  symmetry with a repeat spacing of 63.8 Å. The breadth of the peaks and low scattering intensity at high  $q$  indicates irregular spacing between swollen bilayers, probably due to undulations. The bilayer volume fraction in this sample is estimated to be 0.37 based on the lamellar dilution law for a 23.5 Å bilayer thickness and is close to the maximum swelling limit for this phase, recalling that the solution is micellar at 30 wt %  $\text{DDAHCO}_3$ .

The more concentrated sample exhibits three distinct, broad, peaks, plus a shoulder indicating a weak fourth peak, but these do not index to any known liquid crystalline phase. As only  $L_\alpha$  optical textures were observed under polarizing optical microscopy (Figure 8), this was interpreted as showing coexistence of two distinct  $L_\alpha$  phases. This has previously been identified in both DDAB and DDANO<sub>3</sub>-water binary

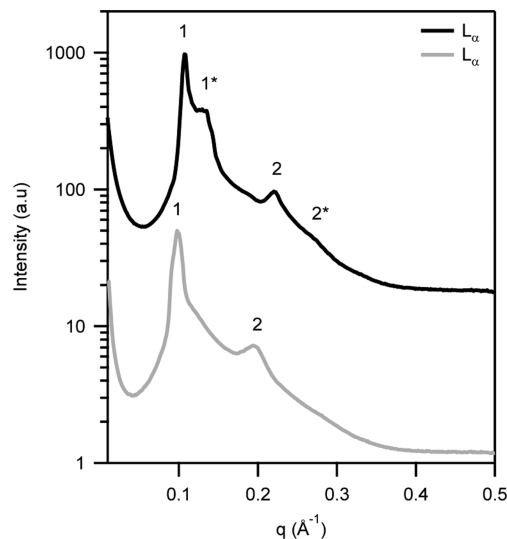


**Figure 8.** SAXS diffraction patterns for the intermediate region within a concentration gradient capillary for  $\text{DDAHCO}_3$ . The concentration increases from bottom to top. The  $L_\alpha$  phase is indicated by the peak ratios 1:2 and 1\*:2\* when two different  $L_\alpha$  structures are in coexistence. Curves are offset for clarity.

systems.<sup>10,12,23</sup> The coexisting phases of  $\text{DDAHCO}_3$  have repeat spacings of 55.1 Å and 44.7 Å. From the dilution law, and assuming the same bilayer thickness as in other  $\text{DDA}^+$  salts investigated here (23.5 Å), these  $\text{DDAHCO}_3$  bilayer spacings correspond to lamellar-lamellar coexistence volume fractions of 0.43 and 0.53. This is quite similar to the 30–70 wt % range in which the lamellar-lamellar coexistence occurs for DDAB.<sup>8</sup>

As expected, the homogeneous  $L_\alpha$  liquid crystalline phase is universally formed in all  $\text{DDA}^+$  surfactants despite the counterion species, at sufficient surfactant concentration. Bilayer structures, including vesicle dispersions, which index 1:2:3... in scattering patterns are formed at much lower concentrations with  $\text{C}_2\text{O}_4^{2-}$  and  $\text{HC}_2\text{O}_4^-$  counterions compared to  $\text{PO}_4^{3-}$ ,  $\text{HPO}_4^{2-}$ ,  $\text{H}_2\text{PO}_4^-$ , and  $\text{HCO}_3^-$  counterions. The periodic spacing between concentrated, collapsed bilayers for the surfactants studied is similar to that of DDAB,<sup>11</sup> and any variations are due to the dimensions of the specific counterion which is affected by hydration and binding strength.

Table 2 summarizes the solubility and self-assembly behavior of  $\text{DDA}^+$  surfactants with various counterions in aqueous solution. “Soluble” salts form an isotropic micellar solution or  $L_1$  phase at concentrations up to several wt %, whereas insoluble salts are characterized by cloudy dilute solutions consisting of vesicle or bilayer dispersions with negligible concentrations of micelles in the continuous phase. At high concentrations the structures revert to the expected lamellar phases, but hydrolyzable ions deliver some unusual features and open a degree of tunability in the aggregates formed.  $\text{HPO}_4^{2-}$  salts are most striking in this regard, yielding two intermediate mesh-like phases, whereas the bicarbonate salt forms, like nitrate and bromide, two distinct lamellar phases.

## CONCLUSIONS

An extensive range of microstructures were found to form in didodecyldimethylammonium ( $\text{DDA}^+$ ) surfactants associated with hydrolyzable phosphate ( $\text{PO}_4^{3-}$ ,  $\text{HPO}_4^{2-}$ , and  $\text{H}_2\text{PO}_4^-$ ), oxalate ( $\text{HC}_2\text{O}_4^-$  and  $\text{C}_2\text{O}_4^{2-}$ ), and bicarbonate ( $\text{HCO}_3^-$ ) counterions. Unlike the corresponding alkyltrimethylammo-

**Table 2. Solubility and Summary of Lyotropic Phases Observed (Denoted X) for Didodecyldimethylammonium (DDA<sup>+</sup>) Surfactants Associated with Various Counterions in Different Hydrolysis States<sup>a</sup>**

anion	L <sub>1</sub>	L <sub>a</sub> <sup>D</sup>	T	L <sub>a</sub>	L <sub>a</sub> '
OH <sup>-</sup> <sup>6,15</sup>	X			X	
CH <sub>3</sub> COO <sup>-</sup> <sup>6</sup>	X			X	
H <sub>2</sub> PO <sub>4</sub> <sup>-</sup>	X	X(?)		X	
HPO <sub>4</sub> <sup>2-</sup>	X	X	X	X	
PO <sub>4</sub> <sup>3-</sup>	X			X	
HCO <sub>3</sub> <sup>-</sup>	X			X	X
SO <sub>4</sub> <sup>2-</sup> <sup>21</sup>				X	
C <sub>2</sub> O <sub>4</sub> <sup>2-</sup>				X	
HC <sub>2</sub> O <sub>4</sub> <sup>-</sup>				X	
Cl <sup>-</sup> <sup>2</sup>				X	
Br <sup>-</sup> <sup>8</sup>				X	X
NO <sub>3</sub> <sup>-</sup> <sup>23</sup>				X	X

<sup>a</sup>(?) denotes a phase observed only by optical microscopy and not confirmed by SAXS.

nium surfactants, the phase behavior is not only different on varying the counterion but also dependent on the hydrolysis state of the counterion species.

DDA<sup>+</sup> phosphates and bicarbonate are highly soluble and form an isotropic phase composed of prolate spheroidal micelles, similar to the dilute solution behavior of DDA<sup>+</sup> hydroxide and acetate. The micelles were found to vary in size depending on the concentration and hydrolysis state of the counterion. In contrast, both DDA<sup>+</sup> oxalates have limited solubility and form large multilamellar vesicles for DDAHC<sub>2</sub>O<sub>4</sub> and a dispersion of poorly swollen vesicles in a dilute micellar solution for DDA<sub>2</sub>C<sub>2</sub>O<sub>4</sub>.

All systems form L<sub>a</sub> phases at high concentration, as expected, but DDA<sub>2</sub>HPO<sub>4</sub> also forms two intermediate mesh phases on the dilute side of a L<sub>a</sub> phase.

Ultimately, the counterions studied can be divided into two groups: very weakly binding counterions (OH<sup>-</sup>, CH<sub>3</sub>COO<sup>-</sup>, PO<sub>4</sub><sup>3-</sup>, HPO<sub>4</sub><sup>2-</sup>, H<sub>2</sub>PO<sub>4</sub><sup>-</sup>, HCO<sub>3</sub><sup>-</sup>) that increase surfactant solubility and form isotropic micellar solution phases and strongly binding counterions (HC<sub>2</sub>O<sub>4</sub><sup>-</sup>, C<sub>2</sub>O<sub>4</sub><sup>2-</sup>, SO<sub>4</sub><sup>2-</sup>, Cl<sup>-</sup>, Br<sup>-</sup>, NO<sub>3</sub><sup>-</sup>) that are sparingly soluble and only form dispersed L<sub>a</sub> structures in dilute solution. The fine control of headgroup geometry and electrostatic interactions that dictate the formation of bilayers, vesicles, meshes, and micelles for DDA<sup>+</sup> surfactants can be designed to be pH sensitive by associating DDA<sup>+</sup> with hydrolyzable phosphate, oxalate, and bicarbonate counterions.

## ASSOCIATED CONTENT

### Supporting Information

Counterion speciation as well as additional SAXS and microscopy characterization of intermediate phases. This material is available free of charge via the Internet at <http://pubs.acs.org>.

## AUTHOR INFORMATION

### Corresponding Author

\*E-mail gregory.warr@sydney.edu.au; Ph (+61 2) 9351 2106 (G.G.W.).

### Notes

The authors declare no competing financial interest.

## ACKNOWLEDGMENTS

We thank Ms. Kanako Sato for preparing samples for SAXS and Dr. Paul Fitzgerald for assistance with the SANS and SAXS experiments. C.K.L. acknowledges receipt of an Australian Postgraduate Award and an AINSE PGRA Scholarship. This research was undertaken on the SAXS/WAXS beamline at the Australian Synchrotron, Victoria, Australia. We acknowledge the support of the National Institute of Standards and Technology, U.S. Department of Commerce, in providing the neutron research facilities used in this work and travel funding from the Access to Major Research Facilities Program.

## REFERENCES

- Israelachvili, J. N.; Mitchell, D. J.; Ninham, B. W. Theory of self-assembly of hydrocarbon amphiphiles into micelles and bilayers. *J. Chem. Soc., Faraday Trans. 2* **1976**, 72, 1525–1568.
- Kunieda, H.; Shinoda, K. Solution behavior of dialkyldimethylammonium chloride in water. Basic properties of antistatic fabric softeners. *J. Phys. Chem.* **1978**, 82 (15), 1710–1714.
- Broxton, T. J.; Sango, X.; Wright, S. Micellar catalysis of organic reactions. 22. A comparison of the basic hydrolysis of benzodiazepinones in the presence of reactive counterion micelles and vesicles. *Can. J. Chem.* **1988**, 66 (7), 1566–1570.
- Ashman, R. B.; Ninham, B. W. Immunosuppressive effects of cationic vesicles. *Mol. Immunol.* **1985**, 22 (5), 609–612.
- Kondo, Y.; Uchiyama, H.; Yoshino, N.; Nishiyama, K.; Abe, M. Spontaneous vesicle formation from aqueous solutions of didodecyldimethylammonium bromide and sodium dodecyl sulfate mixtures. *Langmuir* **1995**, 11 (7), 2380–2384.
- Brady, J. E.; Evans, D. F.; Kachar, B.; Ninham, B. W. Spontaneous vesicles. *J. Am. Chem. Soc.* **1984**, 106, 4279–80.
- Hyde, S. T.; Schroder, G. E. Novel surfactant mesostructural topologies: between lamellae and columnar (hexagonal) forms. *Curr. Opin. Colloid Interface Sci.* **2003**, 8 (1), 5–14.
- Warr, G. G.; Sen, R.; Evans, D. F.; Trend, J. E. Microemulsion formation and phase behavior of dialkyldimethylammonium bromide surfactants. *J. Phys. Chem.* **1988**, 92 (3), 774–783.
- Miller, D. D.; Evans, D. F. Fluorescence quenching in double-chained surfactants. 1. Theory of quenching in micelles and vesicles. *J. Phys. Chem.* **1989**, 93 (1), 323–333.
- Dubois, M.; Zemb, T. Phase behavior and scattering of double-chain surfactants in diluted aqueous solutions. *Langmuir* **1991**, 7 (7), 1352–1360.
- Dubois, M.; Zemb, T.; Belloni, L.; Delville, A.; Levitz, P.; Setton, R. Osmotic-pressure and salt exclusion in electrostatically swollen lamellar phases. *J. Chem. Phys.* **1992**, 96 (3), 2278–2286.
- Caboi, F.; Monduzzi, M. Didodecyldimethylammonium bromide vesicles and lamellar liquid crystal. A multinuclear NMR and optical microscopy study. *Langmuir* **1996**, 12 (15), 3548–3556.
- Patrick, H. N.; Warr, G. G. Counterion binding and regulation of interactions between charged bilayers. *J. Phys. Chem.* **1996**, 100 (40), 16268–16274.
- Miller, D. D.; Magid, L. J.; Evans, D. F. Fluorescence quenching in double-chained surfactants. 2. Experimental results. *J. Phys. Chem.* **1990**, 94 (15), 5921–5930.
- Talmon, Y.; Evans, D. F.; Ninham, B. W. Spontaneous vesicles formed from hydroxide surfactants: Evidence from electron microscopy. *Science* **1983**, 221 (4615), 1047–1048.
- Hashimoto, S.; Thomas, J. K.; Evans, D. F.; Mukherjee, S.; Ninham, B. W. Unusual behavior of hydroxide surfactants. *J. Colloid Interface Sci.* **1983**, 95 (2), 594–596.
- Brady, J. E.; Evans, D. F.; Warr, G. G.; Grieser, F.; Ninham, B. W. Counterion specificity as the determinant of surfactant aggregation. *J. Phys. Chem.* **1986**, 90 (9), 1853–1859.
- Ninham, B. W.; Evans, D. F.; Wei, G. J. The curious world of hydroxide surfactants - Spontaneous vesicles and anomalous micelles. *J. Phys. Chem.* **1983**, 87 (24), 5020–5025.

- (19) Lianos, P.; Zana, R. Micellar properties of alkyltrimethylammonium hydroxides in aqueous solution. *J. Phys. Chem.* **1983**, *87* (8), 1289–1291.
- (20) Jorgensen, W. L.; Gao, J. Monte Carlo simulations of the hydration of ammonium and carboxylate ions. *J. Phys. Chem.* **1986**, *90* (10), 2174–2182.
- (21) Khan, A.; Kang, C. Counterion effects in the self-assembly of didodecyldimethylammonium halides and sulphate surfactants. *Trends Colloid Interface Sci. VII* **1993**, *146*–149.
- (22) Kang, C.; Khan, A. Self-assembly in systems of didodecyldimethylammonium surfactants: Binary and ternary phase equilibria and phase structures with sulphate, hydroxide, acetate, and chloride counterions. *J. Colloid Interface Sci.* **1993**, *156* (1), 218–228.
- (23) Brotons, G.; Dubois, M.; Belloni, L.; Grillo, I.; Narayanan, T.; Zemb, T. The role of counterions on the elasticity of highly charged lamellar phases: A small-angle X-ray and neutron-scattering determination. *J. Chem. Phys.* **2005**, *123* (2), 1–18.
- (24) Dubois, M.; Zemb, T. Swelling limits for bilayer microstructures: the implosion of lamellar structure versus disordered lamellae. *Curr. Opin. Colloid Interface Sci.* **2000**, *5* (1–2), 27–37.
- (25) Liu, C. K.; Warr, G. G. Resiliently spherical micelles of alkyltrimethylammonium surfactants with multivalent, hydrolyzable counterions. *Langmuir* **2012**, *28* (30), 11007–11016.
- (26) Liu, C. K.; Warr, G. G. Hexagonal closest-packed spheres liquid crystalline phases stabilised by strongly hydrated counterions. *Soft Matter* **2014**, *10* (1), 83–87.
- (27) Morini, M. A.; Minardi, R. M.; Schulz, P. C.; Puig, J. E.; Hernández-Vargas, M. E. Basicity of dodecytrimethylammonium hydroxide. *Colloids Surf., A* **1995**, *103* (1–2), 37–40.
- (28) Schulz, P. C.; Morini, M. A.; Minardi, R. M.; Puig, J. E. The aggregation in dodecytrimethylammonium hydroxide aqueous solutions. *Colloid Polym. Sci.* **1995**, *273* (10), 959–966.
- (29) Rosevear, F. B. The microscopy of the liquid crystalline neat and middle phases of soaps and synthetic detergents. *J. Am. Oil Chem. Soc.* **1954**, *31*, 628–39.
- (30) Blackmore, E. S.; Tiddy, G. J. T. Phase behavior and lyotropic liquid crystals in cationic surfactant-water systems. *J. Chem. Soc., Faraday Trans. 2* **1988**, *84* (8), 1115–27 2 plates.
- (31) Hyde, S. T. Identification of Lyotropic Liquid Crystalline Mesophases. In *Handbook of Applied Surface and Colloid Chemistry*; Holmberg, K., Ed.; John Wiley & Sons: New York, 2001; Vols. 1–2, pp 299–321.
- (32) Glinka, C. J.; Barker, J. G.; Hammouda, B.; Krueger, S.; Moyer, J. J.; Orts, W. J. The 30 m Small-Angle Neutron Scattering Instruments at the National Institute of Standards and Technology. *J. Appl. Crystallogr.* **1998**, *31* (3), 430–445.
- (33) Kline, S. Reduction and analysis of SANS and USANS data using IGOR Pro. *J. Appl. Crystallogr.* **2006**, *39* (6), 895–900.
- (34) Munter, A. Scattering length density calculator. <http://www.ncnr.nist.gov/resources/sldcalc.html> (accessed 17.04.11).
- (35) Sears, V. F. Neutron scattering lengths and cross-sections. *Neutron News* **1992**, *3*, 26–37.
- (36) Guinier, A.; Fournet, G. *Small-Angle Scattering of X-Rays*; John Wiley and Sons: New York, 1955.
- (37) Lindner, P.; Zemb, T. *Neutron, X-Ray and Light Scattering: Introduction to an Investigative Tool for Colloid and Polymeric Systems*; Elsevier: North-Holland, Amsterdam, 1991.
- (38) Feigin, L. A.; Svergun, D. I. *Structure Analysis by Small-Angle X-Ray and Neutron Scattering*; Plenum Press: New York, 1987.
- (39) Regev, O.; Kang, C.; Khan, A. Cryo-TEM and NMR studies of solution microstructures of double-tailed surfactant systems: didodecyldimethylammonium hydroxide, acetate, and sulfate. *J. Phys. Chem.* **1994**, *98* (26), 6619–6625.
- (40) Miller, C. A.; Ghosh, O.; Benton, W. J. Behavior of dilute lamellar liquid-crystalline phases. *Colloids Surf.* **1986**, *19* (2–3), 197–223.
- (41) Blom, A.; Warr, G. G.; Wanless, E. J. Growth of double-chained cationic surfactant films on mica. *Aust. J. Chem.* **2006**, *59* (6), 381–385.
- (42) Schulz, J. C.; Warr, G. G.; Butler, P. D.; Hamilton, W. A. Adsorbed layer structure of cationic surfactants on quartz. *Phys. Rev. E* **2001**, *63* (4), 041604.
- (43) Haverd, V. E.; Warr, G. G. Cation selectivity at air/anionic surfactant solution interfaces. *Langmuir* **1999**, *16* (1), 157–160.
- (44) Kekicheff, P.; Tiddy, G. J. T. Structure of the intermediate phase and its transformation to lamellar phase in the lithium perfluorooctanoate/water system. *J. Phys. Chem.* **1989**, *93* (6), 2520–2526.
- (45) Funari, S. S.; Holmes, M. C.; Tiddy, G. J. T. Microscopy, X-ray diffraction, and NMR studies of lyotropic liquid crystal phases in the  $C_{22}EO_6$ /water system: a new intermediate phase. *J. Phys. Chem.* **1992**, *96* (26), 11029–11038.
- (46) Funari, S. S.; Holmes, M. C.; Tiddy, G. J. T. Intermediate lyotropic liquid crystal phases in the  $C_{16}EO_6$ /water system. *J. Phys. Chem.* **1994**, *98* (11), 3015–3023.
- (47) Örädd, G.; Gustafsson, J.; Almgren, M. Intermediate phases in the system egg lecithin/CTAC/brine. SAXS and NMR studies. *Langmuir* **2001**, *17* (11), 3227–3234.
- (48) Ghosh, S. K.; Raghunathan, V. A. Structure of mesh phases in cationic surfactant systems with strongly bound counterions: Influence of the surfactant headgroup and the counterion. *Langmuir* **2009**, *25* (5), 2622–2628.
- (49) Hyde, S. T.; Larsson, K.; Blum, Z.; Landh, T.; Lidin, S.; Ninham, B. W. *The Language of Shape, The Role of Curvature in Condensed Matter: Physics, Chemistry and Biology*; Elsevier Science: Dordrecht, Netherlands, 1997.
- (50) Rinia, H. A.; Demel, R. A.; van der Eerden, J.; de Kruijff, B. Blistering of Langmuir-Blodgett bilayers containing anionic phospholipids as observed by atomic force microscopy. *Biophys. J.* **1999**, *77* (3), 1683–1693.
- (51) Blom, A.; Warr, G. G.; Wanless, E. J. Morphology transitions in nonionic surfactant adsorbed layers near their cloud points. *Langmuir* **2005**, *21* (25), 11850–11855.
- (52) Blom, A.; Duval, F. P.; Kovács, L.; Warr, G. G.; Almgren, M.; Kadi, M.; Zana, R. Direct visualization of mesh structures at solid/solution interfaces by atomic force microscopy. *Langmuir* **2004**, *20* (4), 1291–1297.
- (53) Almgren, M. Mixed micelles and other structures in the solubilization of bilayer lipid membranes by surfactants. *Biochim. Biophys. Acta, Biomembr.* **2000**, *1508* (1–2), 146–163.
- (54) Buchanan, M.; Arrault, J.; Cates, M. E. Swelling and dissolution of lamellar phases: role of bilayer organization. *Langmuir* **1998**, *14* (26), 7371–7377.
- (55) Bergström, M.; Pedersen, J. S.; Schurtenberger, P.; Egelhaaf, S. U. Small-angle neutron scattering (SANS) study of vesicles and lamellar sheets formed from mixtures of an anionic and a cationic surfactant. *J. Phys. Chem. B* **1999**, *103* (45), 9888–9897.
- (56) Hyde, S. T. On swelling and structure of composite materials. Some theory and applications of lyotropic mesophases. *Colloids Surf., A* **1995**, *103* (3), 227–247.
- (57) Guldbrand, L.; Jonsson, B.; Wennerstrom, H.; Linse, P. Electrical double-layer forces - A Monte-Carlo study. *J. Chem. Phys.* **1984**, *80* (5), 2221–2228.
- (58) Underwood, A. L.; Anacker, E. W. Counterion lyotropy and micelle formation. *J. Colloid Interface Sci.* **1987**, *117* (1), 242–250.
- (59) Berr, S.; Jones, R. R. M.; Johnson, J. S. Effect of counterion on the size and charge of alkyltrimethylammonium halide micelles as a function of chain length and concentration as determined by small-angle neutron scattering. *J. Phys. Chem.* **1992**, *96* (13), 5611–5614.
- (60) Aswal, V. K.; Goyal, P. S. Selective counterion condensation in ionic micellar solutions. *Phys. Rev. E* **2003**, *67* (5), 2947–2953.